

To investigate opulence of graphene in ZnO/graphene nanocomposites based dye sensitized solar cells

Bulkesh Siwach¹ · Devendra Mohan¹ · Divya Jyoti²

Received: 26 October 2016 / Accepted: 8 April 2017 / Published online: 24 April 2017
© Springer Science+Business Media New York 2017

Abstract The study reports the application of ZnO–graphene (ZGR) nanocomposite films for Dye-sensitized solar cells (DSSCs) as photoanodes. These nanocomposites were prepared by incorporating different amount of graphene (0–1 wt%) in sol–gel routed ZnO nanoparticles. The presence of graphene in nanocomposite films was revealed by X-ray diffraction (XRD) that was further supported by Field Emission Scanning Electron Microscopy (FESEM) and Energy Dispersive X-ray (EDX). The surface roughness value of these ZGR nanocomposite films was examined by Atomic Force Microscopy (AFM). The UV–Visible spectrum of the synthesized ZGR nanocomposite films was found to be shifted towards a longer wavelength region as compared to bare ZnO that ensured the formation of interfacial contact between ZnO and graphene. The enhanced absorption in the visible region of spectra is observed on incorporation of graphene in these ZGR nanocomposites. Significant increments in room temperature Photoluminescence (PL) intensity was attributed to the plasmonic effect of graphene. DSSCs were assembled with these ZGR nanocomposite photoanode films after tethering with N749 (black dye) and the effect of graphene concentration on their performance was investigated. The maximum power conversion efficiency obtained from these ZGR nanocomposites based DSSC has reached 3.17% that is 53% higher than that of bare ZnO based DSSC (2.07%).

1 Introduction

Solar energy is the most viable source of energy among all sustainable technologies including thermal, tidal, hydropower and biomass. Photovoltaic technology is therefore considered as the most efficient mean of harness solar energy. Though, electricity conversion efficiency values of silicon solar cells are reported to be ~20% but the high manufacturing cost and use of toxic materials in production of purified silicon has inspired the research for the development of low-cost and environmentally benign solar cells [1]. Therefore, an alternate photovoltaic technology is mandatory and there is a need to develop low cost photovoltaic cells for the mass production. Dye-sensitized solar cells (DSSCs) have been recognized as next generation solar technology due to lower production cost, high conversion efficiency, easy manufacturing and eco-friendly nature [2–6]. The fabrication cost of DSSCs is about 1/3 to 1/5 times lower to the cost for silicon solar cells. Though, DSSCs show lower photoconversion efficiency values but have a higher performance to cost ratio in comparison to silicon-based solar cells [7]. DSSC is a 3rd-generation solar cell [5] having capacitive nature that employs high band gap nanostructured semiconductors like TiO₂, ZnO [8, 9], Nb₂O₅, SrTiO₃ [10], SnO₂ [11] and their composites as photoelectrode materials. As ZnO is known to be a wide band gap (3.37 eV) n-type semiconductor that is identical to TiO₂ (3.23 eV) hence similar electron injection actions are expected for both these materials [12] Due to high electron mobility (~107 times more) and lower recombination rate, electron lifetime is considerably higher in ZnO as compared to TiO₂. Moreover, good transparency to visible light, high photo activity and nanocrystalline ZnO of varying morphologies has assumed to be more favorable and potential material for use in DSSCs [13–15]. To improve overall efficiency and stability of DSSCs, several efforts have been made by

✉ Bulkesh Siwach
bulkesh.siwach@gmail.com

¹ Laser Laboratory, Department of Physics, Guru Jambheshwar University of Science & Technology, Hisar 125001, India

² Department of Physics, University College, Faridkot 151202, India

worldwide researchers for developing each component of the device. A few of them involve the usage of solid electrolytes, metal-free dyes, more efficient hole transport materials as well as low cost counter electrode materials [16].

Recently, nanocomposites are one of the major research areas that consist of two or more materials with desired properties primarily because of the synergic effect between those materials that are necessary for various technological applications. Among all the most attractive nanocomposite materials are metal oxides and carbon allotropes. Graphene, one of the carbon allotropes, is a two dimensional material which has attracted global interest due to its remarkable properties such as excellent carrier mobility, superior thermal conductivity, good pore size distribution, high electrical conductivity, capacitive performance and high surface area ($2600 \text{ m}^2\text{g}^{-1}$). It has hexagonal lattice made up of carbon atoms having one-atom thick layer [17–20]. The major drawback of graphene is its zero band gap, but now it is possible to modify its band gap as well as the fermi energy using carrier doping and electrical gating. Currently, researchers have shown an improvement in DSSC efficiency by employing graphene/TiO₂ nanocomposite photoanodes in DSSC fabrication as compared to pure TiO₂ photoanode. The improvement is due to the enhancement of light absorption as larger surface area available for dye impregnation that is associated with a higher transfer rate of photo-generated electrons and suppressed recombination on the electrolyte/photoanode edge [21, 22]. Furthermore, graphene also acts as interfacial layer between photoanode and liquid electrolyte as well as between TiO₂ and transparent conducting oxide (TCO) that diminished back electron transfer. Thus, ZGR nanocomposites are expected to reveal significant improvement in properties such as photocatalytic activity, solar energy conversion as well as energy storage. Thus, the similar performance for ZGR nanocomposite in DSSCs applications is expected [23].

In the present study, ZGR nanocomposites with varying concentration of graphene between 0 and 1 wt% are synthesized and their successful application as photoanodes in DSSCs fabrication is reported. Platinum (Pt) coated ITO is used as counter electrode with iodide based electrolyte and black dye as sensitizer to design the cell. The morphological, structural, compositional, optical and J–V characteristics of the assembled cells are also investigated.

2 Experimental

2.1 Materials

Graphene, Black dye and Indium Tin Oxide glass (ITO) ($15 \Omega \text{ sq}^{-1}$) were procured from Sigma-Aldrich (USA). Polyethylene glycol (PEG) of molecular weight 20,000

was purchased from Himedia (India). De-ionized water was used throughout the experiments to avoid contamination. All the chemicals were used without any further purification.

2.2 Synthesis of ZnO nanopowder and ZnO–graphene nanocomposite photoanodes

The ZnO nanopowder was synthesized via sol–gel process. In short, 0.2 M Zinc acetate dihydrate [$\text{Zn}(\text{CH}_3\text{COO})_2 \cdot 2\text{H}_2\text{O}$] was dissolved in methanol ultrasonically at room temperature to obtain a transparent sol having no precipitate and turbidity. This solution was then mixed to a known quantity of NaOH and stirred ultrasonically for 1 h at room temperature. The sol was then kept undisturbed until white precipitates were obtained. These precipitates were dried at 80 °C after filtering and washing with excess methanol. In order to synthesize ZGR nanocomposites; Graphene powder, ZnO nanopowder, deionized water and PEG₂₀₀₀₀ were grounded together into the mortar with pestle for one and half hours to obtain a fine viscous paste. ZGR nanocomposite films were prepared with graphene having 0, 0.25, 0.5 and 1 wt% and labeled as ZGR0, ZGR0.25, ZGR 0.5 and ZGR1 respectively and were coated on the conducting side of pre-cleaned ITO substrate by doctor-blade method. Before coating the films, substrate was masked using scotch tape to select the active area (0.25 cm^2). These films were dried at room temperature for 10 min and then annealed in a temperature controlled furnace at 450 °C for 30 min. These photoanodes were further immersed in 0.5 mM ethanolic solution of N749 (black dye) for 24 h and excess dye molecules were removed with ethanol.

2.3 Assembling DSSCs

The solar cells were assembled in a sandwich-type structure by putting the dye loaded photoanodes on the top of spin coated Pt counter electrodes. Scotch tape was used as a spacer between the two electrodes of the cell. Iodide-based liquid electrolyte was injected into the devices by capillary action for completing the device. The schematic and energy band diagram of the DSSC based on ZGR nanocomposite film as photoanode are shown in Fig. 1a, b, respectively. Under simulated illumination, electrons from the photoexcited dye are transported to the conduction band (CB) of ZnO and then extracted to ITO via the CB of graphene. Once an electron is injected into the conduction band of ZnO, the photosensitizer dye becomes oxidized. The oxidized dye is regenerated by receiving electrons from the I[−] ion of redox mediator that gets oxidized to I^{−3}. It transports the positive charge to the counter electrode of DSSC. Thus, CB of graphene provides an additional pathway for

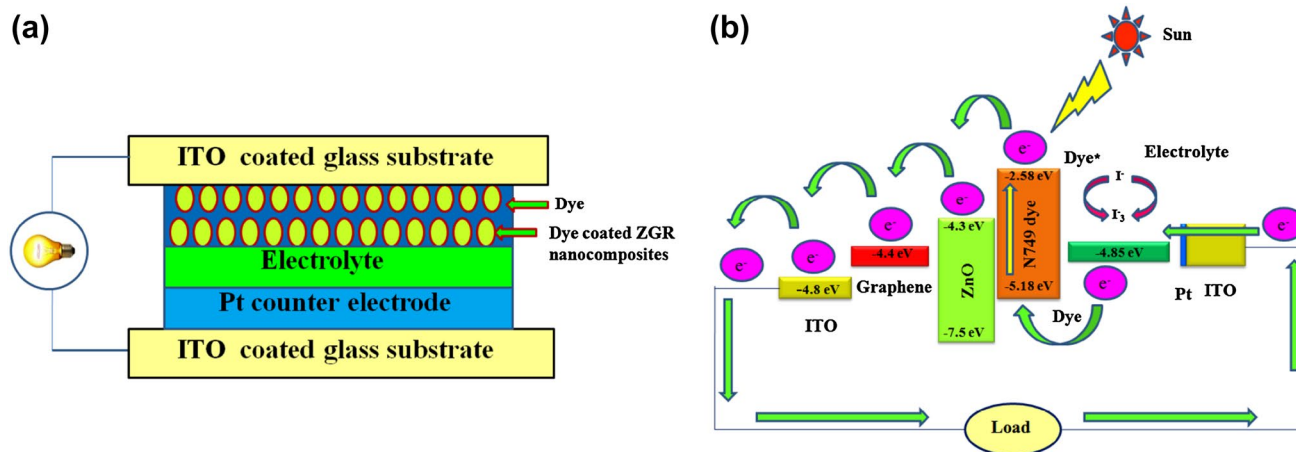


Fig. 1 a Schematics of ZGR based DSSC b Typical energy levels of various components of ZGR based DSSC employing an iodide/triiodide-based redox electrolyte and N749 as a sensitizer

electron transportation in addition to the conventional path in ZGR based DSSC [24]. Moreover, ITO and graphene has similar work functions, -4.8 and -4.4 eV (versus vacuum) respectively, so graphene does not hinder the injected electrons to flow down to the ITO substrate. Therefore, the incorporated graphene in ZGR nanocomposites collects electrons and acts as a transporter layer in the effective charge separation and rapid transportation of the photogenerated electrons which facilitates DSSC to operate more efficiently [25].

2.4 Characterization techniques

The nanocomposite photoanode (without dye) films were structurally characterized by the X-ray diffraction (XRD) using Rikagu Table-Top X-ray diffractometer. Morphological and compositional analysis of these films were carried out by Field emission scanning electron microscopy (FESEM) using TESCAN (model MIRA II LMH) and Energy dispersive X-ray (EDX) from INCA Penta FET \times 3 attached with FESEM. Optical properties of these nanocomposite films were examined by means of UV–Visible absorbance by Varian UV–Vis spectrophotometer (Cary5000) and Photoluminescence spectrophotometer from SHIMADZU (RF-530 Spectro fluorophotometer). The average surface roughness of these nanocomposite films was estimated by Atomic force microscopy (AFM) analysis in tapping mode at the room temperature using NanoScope IIIa SPM. The current density–voltage (J – V) characteristics of the fabricated cells were carried out using a Keithley 2400 Source Meter under simulated sunlight using a SS50AAA (Photo Emission Tech) solar simulator at AM 1.5G (100 mW cm^{-2}). The active area for all the cells was adjusted to be 0.25 cm^2 .

3 Results and discussion

3.1 Structural and phase analysis

Figure 2 shows the XRD patterns of ITO substrate and ZGR nanocomposite films. The diffraction peak corresponding to graphene is observed at $2\theta = 26.8^\circ$ which is assigned to the (002) reflections of graphitic carbon. The intensity of this peak goes on increasing as the graphene concentration increases in nanocomposites. The diffraction peaks attributed to ZnO appears at 2θ values of 31.9° , 34.6° , 36.2° , 47.5° , 56.6° and are indexed to (100), (002), (101), (102), (110) planes respectively of hexagonal wurtzite structure of ZnO [26]. Further, it is observed

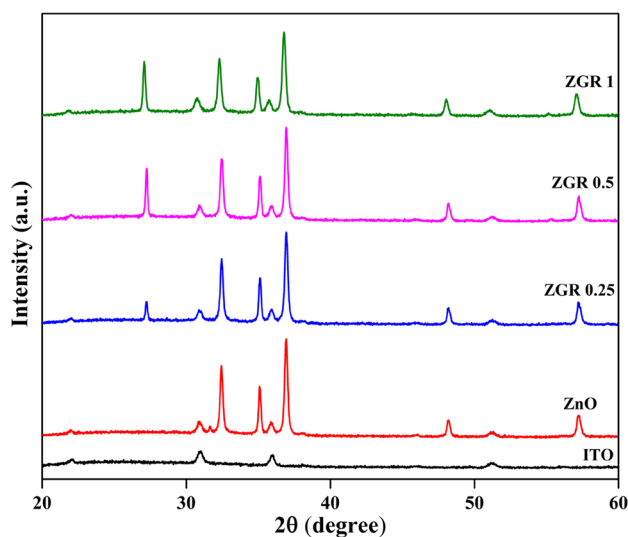


Fig. 2 XRD patterns of ITO substrate, ZnO film (ZGR 0) and ZGR (0.25–1) nanocomposite films

from Fig. 2 that presence of graphene does not cause any changes in preferential orientations of ZnO since all ZGR nanocomposites exhibit similar XRD patterns [27].

3.2 Optical studies

3.2.1 UV–Visible absorption

The optical properties of ZGR nanocomposite films are examined by the UV–Vis absorption spectra as displayed in Fig. 3. Each of these samples shows the characteristic intense light absorption in the UV region of the spectra due to electron promotion of ZnO from the valence band to the conduction band. Moreover, the incorporation of graphene in ZGR nanocomposites increases the light absorption intensity and range in the visible light region as compared to ZnO (ZGR 0) that may be due to modification of the primary process of electron–hole pair creation during irradiation as well as the enhancement of surface electric charge of the oxides in the ZGR nanocomposites [20]. ZGR 0.25 nanocomposite shows maximum absorption in visible region as compared to other competitors that can be clearly noticed from the absorption spectra (Fig. 3). The crystalline quality of the ZnO nanoparticles decorated on graphene surface gets affected as the graphene concentration increases beyond the optimum value of 0.25 wt% (ZGR 0.25). This results in a decrease of ZnO nanoparticles population in ZGR nanocomposites and hence the absorbance in the visible light gradually decreases. These results are in agreement with previous reports in semiconductor/graphene nanocomposites [28, 29]. Therefore, considerable influence of graphene concentration on the optical

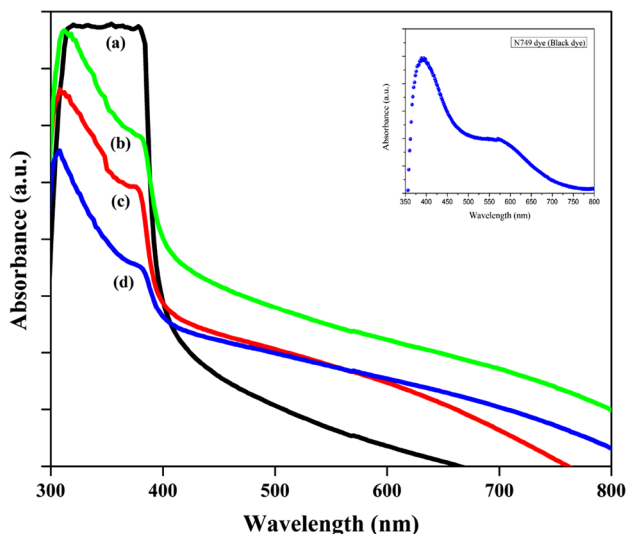


Fig. 3 UV–Visible absorption spectra of (a) ZGR 0 (b) ZGR 0.25 (c) ZGR 0.5 and (d) ZGR 1 nanocomposite films. *Inset* of the figure shows absorption spectra of N749 dye in ethanol

properties of these ZGR nanocomposites is observed. The visible-light photocatalytic activity of ZnO improves with incorporation of graphene in ZnO matrix. It can be noticed from Fig. 3 that absorption edge of ZGR nanocomposites is shifted towards a higher wavelength region as compared to ZGR 0, indicating a reduction in band gap that is linked to the chemical action between ZnO and graphene such as formation of C–O–Zn bonds [20, 30]. Herein, N749 dye (black dye) is employed as a sensitizer in DSSCs. The absorption spectrum of the dye dissolved in ethanol is shown in Inset of Fig. 3. The dye under reference shows broad and intense visible bands in the 390–600 nm regions due to metal-to-ligand charge transfer transitions [31]. Therefore, after tethering the ZGR nanocomposite films with N749 dye, the broadening of absorption spectra takes place that is advantageous for harvesting the solar spectrum and generates a higher photocurrent. Furthermore, The Tauc equation is employed to find out the band gap of semiconductors that can be written as follows [32]:

$$\alpha h\nu = \text{constant} (h\nu - E_g)^n \quad (1)$$

Here E_g is the optical band gap, n equals $\frac{1}{2}$ for direct transition, and equals 2 for indirect transition, α is calculated as $2.303 A/d$, A is the optical density and d is the thickness of the sample. The thickness of all the samples is found to be $9 \mu\text{m}$ as measured by digital micrometer screw gauge having least count $1 \mu\text{m}$. The Tauc plots of all ZGR nanocomposite films are represented in Fig. 4. The direct band gap energies predicted from the intercept of the tangents to the plots are about 3.18, 3.05, 3.14 and 3.09 eV approximately, corresponding to ZGR 0, ZGR 0.25, ZGR 0.5 and ZGR 1, respectively. It is found that the estimated band gap values decrease with the incorporation of graphene in ZGR nanocomposites, which could be due to synergistic interfacial contact between the ZnO and graphene [23, 33]. The qualitative observation of a red shift in the absorption edge of ZGR nanocomposites as compared to bare ZnO is also supported by these results.

3.2.2 PL studies

Figure 5 illustrates the PL spectra of the ZGR nanocomposite films recorded at room temperature using $\sim 325 \text{ nm}$ as the excitation wavelength. Due to having lesser PL intensity as compared to other samples, the PL spectra of ZGR 0 film is shown in inset of Fig. 5. All the samples exhibit similar PL peaks. The emission peaks centered at 415 and 439 nm are assigned to band-to-band transitions and the zinc vacancy associated with defect states, respectively. The visible emission peaks at 468 and 494 nm are attributed to different deep level defect states arising from the zinc interstitials and oxygen vacancies present in ZnO

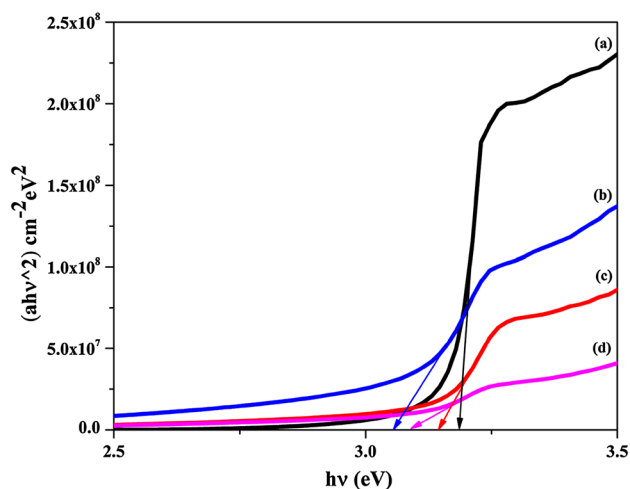


Fig. 4 Tauc Plot of (a) ZGR 0 (b) ZGR 0.25 (c) ZGR 0.5 and (d) ZGR 1 nanocomposite films

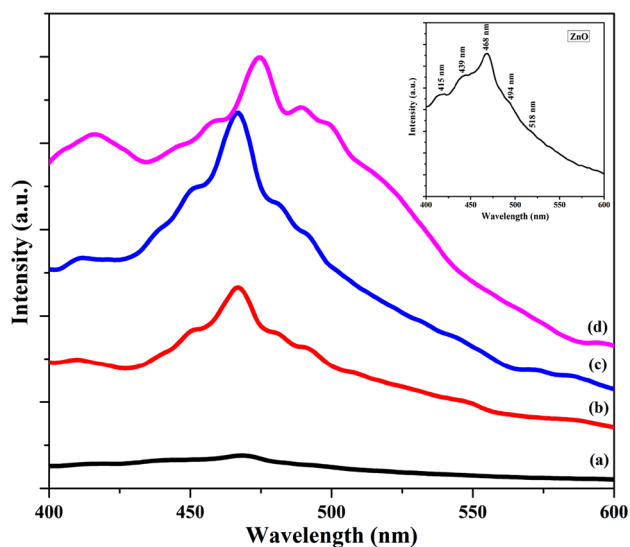


Fig. 5 PL spectra of (a) ZGR 0 (b) ZGR 0.25 (c) ZGR 0.5 and (d) ZGR 1 nanocomposite films. Inset of the figure shows PL spectrum of bare ZnO film (ZGR 0)

lattice [23, 34]. A deep level peak at 518 nm in green emission is attributed to zinc vacancies [20, 35]. Also a small red shift is observed in PL peak positions as the concentration of graphene increases in these ZGR nanocomposites, which is understood to be related to the interaction between graphene and ZnO nanoparticles [36]. From Fig. 5, it can be seen that PL intensity of ZGR 0.25, ZGR 0.5 and ZGR 1 nanocomposite films is much higher than that of ZGR 0 nanocomposite film and these results are in well agreement with previous reports [37]. Hence, it is inferred that the plasmonic effect of graphene have some involvement in the improvement of the photocurrent in the ZGR based DSSC

showing that graphene is a promising material to be applied in optoelectronic devices in visible as well as ultraviolet frequency region [8].

3.3 Morphological analysis

The FESEM images shown in Fig. 6 depict the morphologies of ZGR 0, ZGR 0.25, ZGR 0.5 and ZGR 1 nanocomposite films. It is seen from these images that these films are having porous and rough morphology. Rice like structures of ZnO are formed as observed from Fig. 6a. It is observed from the FESEM analysis that ZGR 0.25 based electrode (Fig. 6b) possesses higher porosity as compared to the electrode fabricated using ZGR 0 and more porosity would result in the enhancement of the surface area that lead to more dye adsorption and the improvement of the photoelectric properties of electrode fabricated from ZGR 0.25 nanocomposite [22, 38]. Moreover, the porosity increases and aggregation starts with increase in concentrations of graphene such as in ZGR 0.5 and ZGR 1, as shown in Fig. 6c–d that in turn provides a way for electrolyte to reach substrate and consequently efficiency falls down.

3.4 Compositional analysis

Figure 7a–d shows the EDX spectrum of ZGR 0, ZGR 0.25, ZGR 0.5 and ZGR 1 nanocomposite films, respectively. Carbon peak in these ZGR nanocomposites is easily identified which confirms the presence of graphene in the ZnO matrix. The spectrum also contains peaks of gold (Au) because of its coating done prior to the EDX measurement and, no other impurity is detected in these ZGR nanocomposites films except coating element Au, confirming the purity of films.

3.5 AFM studies

The AFM images of ZGR 0, ZGR 0.25, ZGR 0.5 and ZGR 1 nanocomposite films are shown in Fig. 8a–d, respectively. The selected scanning size is $2\ \mu\text{m} \times 2\ \mu\text{m}$ for all the samples. The average roughness of ZGR 0, ZGR 0.25 and ZGR 1 is found to be 89.41, 115.32, 98.61 and 96.72 nm, respectively. Hence, the average roughness is found to be increased in ZGR nanocomposite films as compared to bare ZnO (ZGR 0) with the maximum value in ZGR 0.25. It is known that the low roughness factors are shown by the high-crystalline composite materials. The highest roughness factor of ZGR 0.25 nanocomposite film is attributed to the decreased crystallinity in comparison with ZGR 0.5 and ZGR 1 nanocomposite films [39, 40]. Moreover, Mahalingam et al. [41] reported that due to the decrease in the photon reflecting angle, a rough surface film will increase the photon conversion

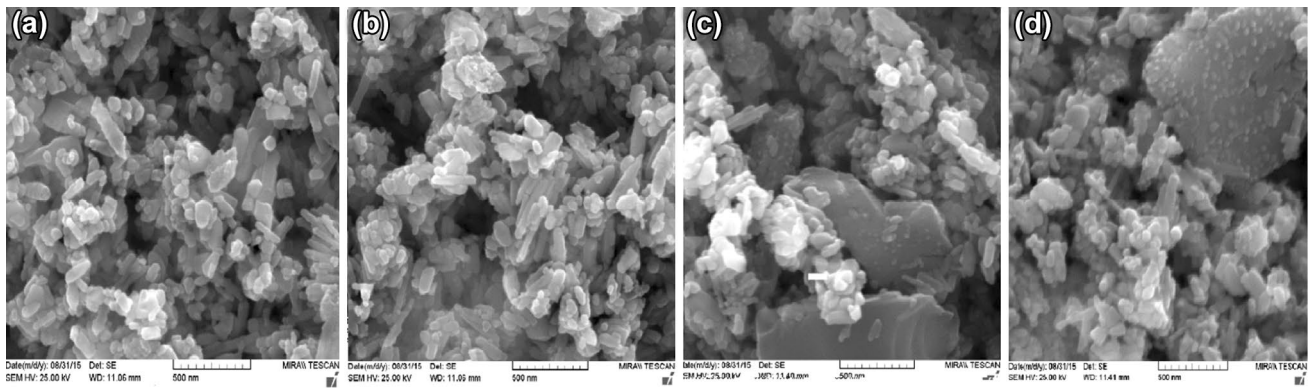


Fig. 6 FESEM images of **a** ZGR 0 **b** ZGR 0.25 **c** ZGR 0.5 and **d** ZGR 1 nanocomposite films

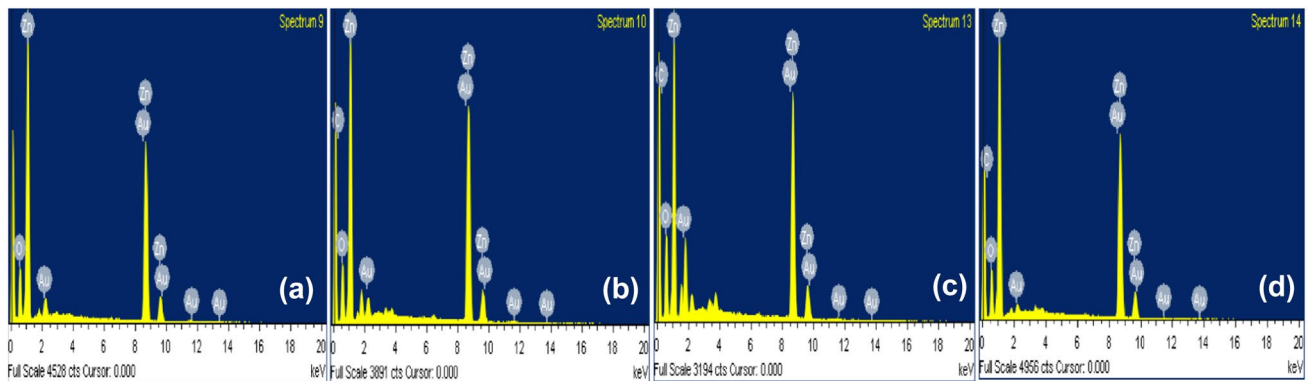


Fig. 7 EDX spectrum of **a** ZGR 0 **b** ZGR 0.25 **c** ZGR 0.5 and **d** ZGR 1 nanocomposite films

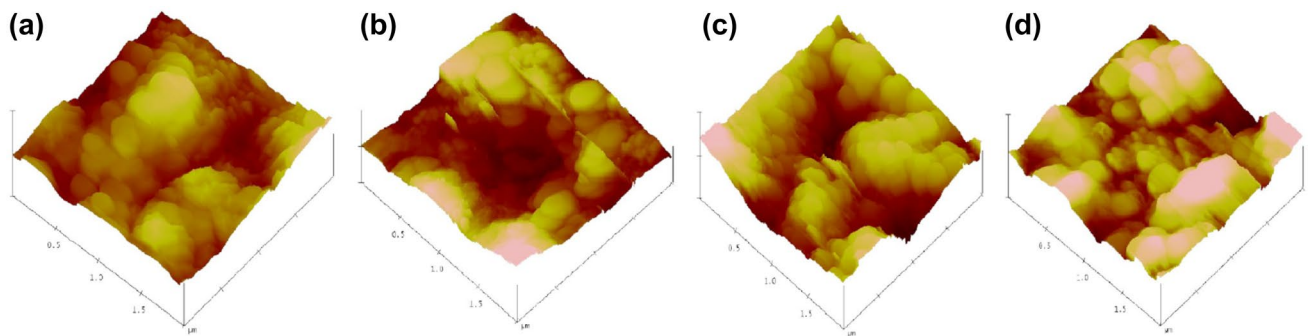


Fig. 8 AFM images of **a** ZGR 0 **b** ZGR 0.25 **c** ZGR 0.5 and **d** ZGR 1 nanocomposite films

efficiency of DSSCs. This is because a higher rough surface will facilitate the photon to bounce on the film surface, particularly due to its greater angle on the surface texture of the film. As a result, the photon will indirectly bounce back to the surface of the film and improve the photon absorption.

3.6 Photocurrent density–voltage (J–V) characteristics

The typical photocurrent density–voltage (J–V) curves of the DSSCs fabricated with ZGR nanocomposite photoanodes having active area of 0.25 cm² measured by solar simulator with AM 1.5G (100 mW cm⁻²) are compared in

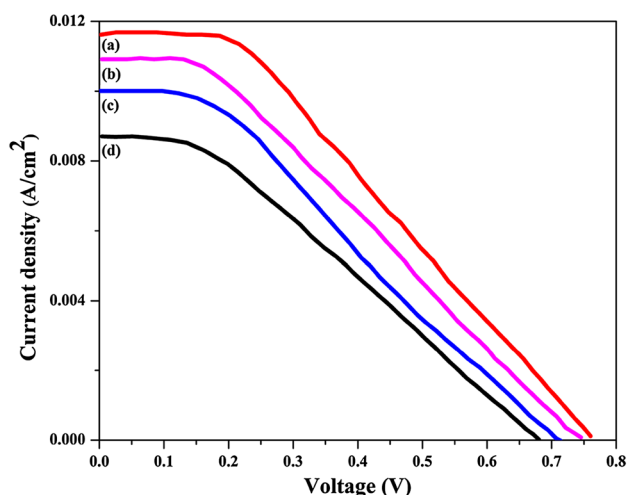


Fig. 9 J–V curves of DSSCs based on (a) ZGR 0.25 (b) ZGR 0.5 (c) ZGR 1 and (d) ZGR 0 nanocomposite films

Table 1 Photovoltaic performance of ZGR nanocomposite photoanode based DSSCs calculated from J–V curves

Sample	J_{SC} (mA cm ⁻²)	V_{OC} (V)	FF	η (%)
ZGR 0	8.7	0.68	0.35	2.07
ZGR 0.25	11.6	0.76	0.36	3.17
ZGR 0.5	10.9	0.74	0.31	2.50
ZGR 1	9.0	0.71	0.38	2.42

Fig. 9. The fill factor (FF) and conversion efficiency (η) of the cell are estimated as [42]:

$$FF = \frac{J_{max} V_{max}}{J_{SC} V_{OC}} \tag{2}$$

$$\eta = \frac{FF J_{SC} V_{OC}}{P_{in}} \tag{3}$$

where I_{max} , V_{max} , I_{SC} , V_{OC} and P_{in} represents the maximum value of output current, maximum value of output voltage, the short-circuit current, open-circuit voltage and the

energy of incident photon, respectively. The photovoltaic parameters of these DSSCs viz. Fill factor (FF), open circuit voltage (V_{OC}) and photocurrent density (J_{SC}) are summarized in Table 1. It is observed from the Table 1 that there is an increase in J_{SC} and η (maxima in case of ZGR 0.25) in DSSCs made with ZGR nanocomposites as compared to bare ZnO (ZGR 0) photoanode. The incorporation of graphene in the ZnO matrix causes quicker electron transport kinetics as graphene has very high carrier mobility of the order of 10^4 cm² V⁻¹ s⁻¹ at room temperature. Under irradiation, the photoinjected electrons on the conduction band of ZnO are trapped by the graphene sheets that could efficiently separate the photo-induced electrons and prevents the charge recombination thereby enhancing the photocatalytic performance of DSSCs based on ZGR nanocomposite photoanodes. Actually, the electronic interaction between ZnO and graphene improves the charge separation efficiency of these ZGR nanocomposites [27–29]. However, to generate a high photocurrent density, the optimum concentration of graphene is a key factor and need to be considered. Thus, when the graphene content in ZGR nanocomposites increases beyond its optimum value (ZGR 0.25), DSSC efficiency falls down (Table 1). This reduction in DSSCs efficiency can be credited to two reasons: (a) with the increase in the graphene concentration further, there exist a light yielding competition between the ZnO, dye and graphene due to absorption of some UV light as well as light in a broad wavelength range of 200–800 nm by graphene. Therefore, light absorption by the sensitizer dye was decreased as the ZnO was surrounded by graphene. (b) the excessive graphene content behave as a type of recombination center that accelerates recombination of electrons to the dye or back reaction to the electrolyte. Hence, all of these factors lead to decrease of the photocatalytic performance of DSSC [27]. Therefore, all the factors discussed in above paragraphs regarding porosity, PL spectra, morphology etc. favors ZGR 0.25 to be used as photoanode in DSSC and efficiency values obtained support the results discussed already.

Table 2 summarizes the comparison of the obtained efficiency value of the present study with the previous

Table 2 Comparison of the energy conversion efficiency of ZGR based DSSCs with the previous studies reported in references [14, 43, 44]

DSSC's Parameters	Hsu et al. [18]		Song et al. [43]		Chang et al. [44]		Present study	
	ZnO/TiO ₂	Graphene/ZnO/TiO ₂	Pure ZnO	rGO/ZnO	Pure ZnO	Graphene/ZnO	Bare ZnO	ZGR 0.25
J_{SC} (mA cm ⁻²)	11.3	17.5	3.58	6.77	6.71	9.20	8.7	11.6
V_{OC} (V)	0.45	0.5	0.60	0.63	0.63	0.61	0.68	0.76
FF	0.47	0.45	0.53	0.60	0.72	0.65	0.35	0.36
η (%)	2.4	3.9	1.14	2.58	3.06	3.67	2.07	3.17

studies reported in references [18, 43, 44]. These previous reports imply that the performance of DSSC can be improved with the addition of graphene in ZnO matrix. The Table 2 shows small variations in DSSC efficiency values due to the different sensitizer and photoanode fabrication methods employed such as spin coating [18] and doctor blade method [43, 44]. In present study, ZGR nanocomposite photoanodes were coated by doctor blade method that showed the conversion efficiency of 3.17%. The improvement of photovoltaic properties of DSSC by the introduction of the ZGR nanocomposite film as photoanode is attributable to the strong adsorption of dye due to increased surface area of the film and reduction of electron recombination. The future work would consider optimization of parameters for further improvement in efficiency of DSSCs.

4 Conclusions

We have successfully synthesized and employed ZGR nanocomposites as photoanodes in DSSC fabrication. A significant increase in the J_{SC} , FF, V_{OC} and η is observed in ZGR 0.25 based DSSC as compared to ZGR 0 showing the effect of graphene content incorporation in ZnO matrix on the efficiency of DSSCs. The ZnO nanoparticles present on the surface of the flat graphene makes more surface area available for higher loading of dye molecules on the surface of the ZnO nanoparticles and consequently increases the DSSCs performance parameters. As the amount of graphene is increased to 1 wt % (ZGR 1), then it is understood that the active ZnO sites available for electron transport also reduced thereby reducing the overall efficiency.

Acknowledgements The authors are grateful to UGC-SAP, New Delhi (DRS-II) and Department of Physics and Astrophysics, Delhi University (New Delhi) for providing XRD and J–V characteristics, respectively. Authors are also grateful to IUAC (an autonomous centre of UGC) for providing FESEM, EDX and AFM facility.

Compliance with Ethical Standards

Conflict of interest We hereby declare that we have no conflict of interest.

References

- S. Suhaimi, M.M. Shahimin, Z.A. Alahmed, J. Chysky, A.H. Reshak, *Int. J. Electrochem. Sci.* **10**, 2859 (2015)
- C.E. Cheng, C.Y. Lin, C.H. Shan, S.Y. Tsai, K.W. Lin, C.S. Chang, F.S.S. Chien, *J. Appl. Phys.* **114**, 014503 (2013)
- H. Elbohy, A. Aboagye, S. Sigdel, Q. Wang, M.H. Sayyad, L. Zhang, *J. Mater. Chem. A* **3**, 17721 (2015)
- D. Jyoti, D. Mohan, R. Dhar, *Mod. Phys. Lett. B* **26**, 1250123 (2012)
- F.I. Lai, J.F. Yang, S.Y. Kuo, *Materials* **8**, 8860 (2015)
- D. Jyoti, D. Mohan, R. Dhar, *J. Renew. Sustain. Energy* **5**, 013112 (2013)
- B. O'Regan, M. Grätzel, *Nature* **353**, 737 (1991)
- G. Khurana, S. Sahoo, S.K. Barik, S.R. Katiyar, *J. Alloys Compd.* **578**, 257 (2013)
- M. Kaur, N.K. Verma, *J. Mater. Sci.* **24**, 3617 (2013)
- F. Lenzenmann, J. Krueger, S. Burnside, K. Brooks, M. Grätzel, D. Gal, S. Rühle, D. Cahen, *J. Phys. Chem. B* **105**, 6347 (2001)
- D.N. Srivastava, S. Chappel, O. Palchik, A. Zaban, A. Gedanken, *Langmuir* **18**, 4160 (2002)
- S.A. Patilab, H.J. Hwanga, M.H. Yua, N.K. Shresthac, S.H. Kim, *RSC Adv.* **7**, 6565 (2017)
- O. Lupan, V.M. Guerin, L. Ghimpu, I.M. Tiginyanu, T. Pauporte, *Chem. Phys. Lett.* **550**, 125 (2012)
- E.M.C. Fortunato, P.M.C. Barquinha, A.C.M.B.G. Pimentel, A.M.F. Goncalves, A.J.S. Marques, L.M.N. Pereira, R.F.P. Martins, *Adv. Mater.* **17**, 590 (2005)
- A.R. Rao, V. Dutta, *Nanotechnology* **19**, 445712 (2008)
- M.S.H. Choudhury, N. Kishi, T. Soga, *Jpn. J. Appl. Phys.* **55**, 01AA16 (2016)
- A.R. Marlinda, N.M. Huang, M.R. Muhamad, M.N. Anam, B.Y.S. Chang, N. Yusoff, I. Harrison, H.N. Lim, C.H. Chia, S.V. Kumar, *Mater. Lett.* **80**, 9 (2012)
- C.H. Hsu, C.C. Lai, L.C. Chen, P.S. Chan, *J. Nanomater.* **2014**, 748319 (2014)
- N. Zhao, X. Cheng, Y. Zhou, M. Yang, J. Yang, T. Zhong, S. Zheng, *J. Nanopart. Res.* **16**, 2335 (2014)
- R. Lv, X. Wang, W. Lv, Y. Xu, Y. Ge, H. He, G. Li, X. Wu, X. Li, Q. Li, *J. Chem. Technol. Biotechnol.* **90**, 550 (2015)
- S. Sun, L. Gao, Y. Liu, *Appl. Phys. Lett.* **96**, 083113 (2010)
- X. Fang, M. Li, K. Guo, Y. Zhu, Z. Hu, X. Liu, B. Chen, X. Zhao, *Electrochim. Acta.* **65**, 174 (2012)
- P. Jayabal, S. Gayathri, V. Sasirekha, J. Mayandi, V. Ramakrishnan, *J. Nanopart. Res.* **16**, 2640 (2014)
- S.P. Lim, P. A., N.M. ikumar, Huang, N.H. Lim, *Int. J. Energy Res.* **39**, 812 (2015)
- F. Xu, J. Chen, X. Wu, Y. Zhang, Y. Wang, J. Sun, H. Bi, W. Lei, Y. Ni, L. Sun, *J. Phys. Chem. C* **117**, 8619 (2013)
- X. Dong, Y. Cao, J. Wang, M.B. Chan-Park, L. Wang, W. Huang, P. Chen, *RSC Adv.* **2**, 4364 (2012)
- X. Liu, L. Pan, T. Lv, T. Lu, G. Zhu, Z. Suna, C. Sunb, *Catal. Sci. Technol.* **1**, 1189 (2011)
- M. Azarang, A. Shuhaimi, R. Yousefi, M. Sookhikian, *J. Appl. Phys.* **116**, 084307 (2014)
- S. Gayathri, P. Jayabal, M. Kottaisamy, V. Ramakrishnan, *J. Appl. Phys.* **115**, 173504 (2014)
- B. Weng, M.Q. Yang, N. Zhang, Y.J. Xu, *J. Mater. Chem. A* **2**, 9380 (2014)
- M. Akhtaruzzaman, A. Islam, M.R. Karim, A.K.M. Hasan, L. Han, *J. Chem.* **2013**, 5 (2013)
- J. Tauc, R. Grigorovici, A. Vancu, *Phys. Status Solidi* **15**, 627 (1966)
- Z. Chen, N. Zhang, Y.J. Xu, *CrystEngComm* **15**, 3022 (2013)
- K.S. Babu, A.R. Reddy, C. Sujatha, K.V. Reddy, *Mater. Lett.* **99**, 97 (2013)
- F.E. Ghodsi, H. Absalan, *Acta Phys. Polonica A* **118**, 659 (2010)
- R. Sharma, F. Alam, A.K. Sharma, V. Dutta, S.K. Dhawan, *J. Mater. Chem. C* **2**, 8142 (2014)
- S.W. Hwang, D.H. Shin, C.O. Kim, S.H. Hong, M.C. Kim, J. Kim, *Phys. Rev. Lett.* **105**, 127403 (2010)
- M. Kaur, N.K. Verma, *J. Mater. Sci.* **24**, 4980 (2013)
- T.H. Tsai, S.C. Chiou, S.M. Chen, *Int. J. Electrochem. Sci* **6**, 3333 (2011)
- M.S. Akhtar, J.G. Park, H.C. Lee, S.K. Lee, O.B. Yang, *Electrochim. Acta.* **55**, 2418 (2010)

41. S. Mahalingam, H. Abdullah, I. Ashaari, S. Shaari, A. Muchtar, J. Phys. D. **49**, 075601 (2016)
42. S. Ananth, T. Arumanayagam, P. Vivek, P. Murugakoothan, J. Mater. Sci. **27**, 146 (2016)
43. J.L. Song, X. Wang, Physica E Low Dimens. Syst. Nanostruct. **81**, 14 (2016)
44. W.C. Chang, T.C. Tseng, W.C. Yu, Y.Y. Lan, M.D. Ger, J. Nanosci. Nanotechnol. **16**, 9160 (2016)